

Quantum Signatures in the Quantum Carnot Cycle

Roie Dann

The Institute of Chemistry, The Hebrew University of Jerusalem, Jerusalem 9190401, Israel

Kavli Institute for Theoretical Physics, University of California, Santa Barbara, CA 93106, USA

E-mail: roie.dann@mail.huji.ac.il

Ronnie Kosloff

The Institute of Chemistry, The Hebrew University of Jerusalem, Jerusalem 9190401, Israel

Kavli Institute for Theoretical Physics, University of California, Santa Barbara, CA 93106, USA

E-mail: ronnie@fh.huji.ac.il

August 2019

Abstract. The Carnot cycle combines reversible isothermal and adiabatic strokes to obtain optimal efficiency, at the expense of a vanishing power output. Quantum Carnot-analog cycles are constructed and solved, operating irreversibly at non-vanishing power. Swift thermalization is obtained in the isotherms utilizing a shortcut to equilibrium protocols and the adiabats employ frictionless unitary shortcuts. The working medium in this study is composed of a particle in a driven harmonic trap. For this system, we solve the dynamics employing a generalized canonical state. Such a description incorporates both changes in energy and coherence. This allows comparing three types of Carnot-analog cycles, Carnot-shortcut, Endo-shortcut and Endo-global. The Carnot-shortcut engine demonstrates the trade-off between power and efficiency. It poses a maximum in power, a minimum cycle time where it becomes a dissipator and for a diverging cycle time approaches the ideal Carnot efficiency. The irreversibility of the cycle arises from non-adiabatic driving, which generates coherence. To study the role of coherence we compare the performance of the shortcut cycles, where coherence is limited to the interior of the strokes, with the Endo-global cycle where the coherence never vanishes. The Endo-global engine exhibits a quantum signature at a short cycle-time, manifested by a positive power output while the shortcut cycles become dissipators. If energy is monitored the back action of the measurement causes dephasing and the power terminates.

1. Introduction

In 1824 Sadi Carnot envisioned a reversible reciprocating heat engine, composed of two adiabatic and two isothermal strokes. He argued that such a reversible engine is universal, and produces optimal work, depending only on the hot and cold bath temperatures, T_h and T_c [1]. This cycle is termed Carnot cycle and serves as a template for all reversible engines. Generally, a heat engine transforms heat extracted from a hot bath, Q_h , to work W . According to the second law of thermodynamics this work is necessarily accompanied by a heat flow to the cold bath $Q_c = |W| - Q_h$. The efficiency of the energy transformation is defined by $\eta = -W/Q_h$, which is bounded by the Carnot cycle efficiency $\eta < \eta_C = 1 - T_c/T_h$, for any heat cycle. This universal bound depends only on the bath temperatures, irrespective of the specific working medium. It translates a fundamental limitation, the second law of thermodynamics, to a practical operational limit applying to all engines. Optimal efficiency is achieved only for a reversible operation.

Practically, any finite power engine operates under irreversible conditions, which leads to a trade-off between efficiency and power. This relation has been extensively studied in the framework of finite-time thermodynamics [2, 3]. A prominent emerging result states that under endoreversible conditions the efficiency at maximum power is given by the Curzon-Ahlborn-Novikov efficiency $\eta_{CAN} = 1 - \sqrt{T_c/T_h}$ [4, 5], which has been generalized for weak dissipation [6, 7].

In the quantum regime energy transfer is constrained as well by the second law of thermodynamics [8, 9, 10, 11]. Implying that quantum heat engines are also bounded by the Carnot efficiency. Reversibility and optimal efficiency is obtained in the quantum adiabatic limit, requiring an infinite cycle-time τ_{cycle} .

In this paper we explore two quantum approaches to obtain non-vanishing power for a ‘Carnot-analog’ engine. The first type is termed *Carnot-shortcut*, defined by the cycle parameters of the reversible Carnot cycle (bath temperatures and external parameters). At the switching corners between strokes, the working medium is in equilibrium with the baths and out of equilibrium at intermediate times (Fig. 1 Panel (a)). Finite power is achieved by shortcut protocols to each stroke: Shortcuts To Adiabaticity (STA) [12] on the unitaries and Shortcut To Equilibrium (STE) [13] for the thermalization strokes. The cycle is performed by external driving of the system and coupling/decoupling the Working Medium (WM) from the hot and cold baths. Typically, the WM Hamiltonian does not commute with itself at different times $[\hat{H}_S(t), \hat{H}_S(t')] \neq 0$, leading to generation of coherence and an accompanied cost in work [14, 15, 16].

An alternative approach to obtain finite power is a *Quantum Endoreversible* cycle (second type of ‘Carnot analog’ engine), for which the WM is in a non-equilibrium state throughout the cycle. In the class of endoreversible cycles, we construct the *Endo-shortcut* and the *Endo-global* cycles, which are characterized by *Branch* and *Global* coherence operations, respectively. Branch coherence is restricted to the interior of the stroke, while at the cycle’s four corners the coherence vanishes and the WM state

is of a Gibbs form, with an internal temperature $T \neq T_{bath}$. In the global coherence operation the WM state exhibits coherence throughout the whole cycle. As a result, coherence generated in one stroke continues to play a role in the subsequent strokes.

Our current aim is to explore the performance and characteristics of the Quantum Carnot-analog engines, i.e., the trade-off between power and efficiency and the role of quantum coherence in the engine operation. For this purpose, we employed an harmonic oscillator WM, allowing an explicit solution of the cycle dynamics. Recently, such a working medium has been employed to experimentally realize quantum heat engines [17, 18].

Previous studies of the Carnot cycle lacked coherence. These studies consider a Hamiltonian that commutes with itself at all times [19, 20], or cycles performed in the adiabatic [21, 22] or stochastic [6] limits. The relatively few studies on the quantum Carnot-analog cycle is in contrast to the popularity of the quantum Otto cycle. Analysis of the Otto cycle has been a major source of insight on quantum reciprocating engines [14, 23, 24, 25, 17, 26, 27, 28, 29, 30, 31, 32, 33, 34, 35]. The vast difference in popularity between the quantum Otto and Carnot cycles arises from the difficulty to describe the open-system dynamics of non-adiabatically driven systems. Recent development of the Non-Adiabatic Master Equation (NAME) [36] and the inertial theorem [37] enable this study.

The analysis of the quantum Carnot-analog engine, demonstrates two roles of coherence in the energy representation. First, the control of coherence allows optimizing the efficiency for a finite cycle-time, minimizing quantum friction [14]. Moreover, for very short cycle-times global coherence becomes crucial to obtain non-vanishing power. This phenomena is a quantum signature [38, 39, 40], which can be unraveled from thermodynamics observables. We consider a thermodynamic quantum signature as a measurable thermodynamic quantity, such as work or efficiency, which indicates a unique quantum behaviour. Such behaviour, by definition, does not have a classical counterpart. Specifically, we find that under fast driving the coherent work extraction mechanism outperforms the stochastic work extraction [38].

The paper is organized as follows: We begin by addressing the general construction and features of the various Carnot analog cycles, Sec 2. Section 3 then focuses on the Carnot-shortcut cycle, describing its construction and thermodynamics behaviour. In this framework, we discuss the role of coherence in the efficiency-power tradeoff, which naturally emerges in the performance of the Carnot-shortcut cycle. In Sec. 4 we introduce two additional Carnot analog cycles, the endoreversible shortcut and global Carnot cycles. Following the description, we compare between branch and global coherence operation modes, associated with these two cycles. Such comparison, highlights the role of coherence in the fast driving regime, and illuminates the emergence of quantum thermodynamics signatures. We conclude in Sec. 5 with a summary and compare the quantum Carnot and Otto engines.

2. Dynamics of the Carnot-analog cycle

We choose a particle of mass m confined by a varying Harmonic potential as the engine's working medium. The associated Hamiltonian reads

$$\hat{H}(t) = \frac{\hat{P}^2}{2m} + \frac{1}{2}m\omega^2(t)\hat{Q}^2, \quad (1)$$

where \hat{Q} and \hat{P} are the position and momentum operators, and $\omega(t)$ is the oscillator frequency and the control parameter. The explicit time-dependence of $\omega(t)$ defines the cycle's protocol.

The dynamics during the cycle strokes is associated with a time-dependent completely positive map [41, 42], generated by

$$\frac{d\hat{\rho}(t)}{dt} = \mathcal{L}(t)\hat{\rho}(t), \quad (2)$$

For the adiabatic strokes $\mathcal{L}(t)\hat{\rho}(t) = -i[\hat{H}(t), \hat{\rho}(t)]$, generating the unitary maps of the adiabatic expansion and compression \mathcal{U}_{ch} and \mathcal{U}_{hc} .

In the isothermal-type strokes $\mathcal{L}(t)\hat{\rho}(t) = -i[\hat{H}(t), \hat{\rho}(t)] + \mathcal{L}_D(t)\hat{\rho}(t)$, where $\mathcal{L}_D(t)$ is an explicitly time-dependent Lindbladian [36], generating the isotherms dynamical maps, \mathcal{U}_h and \mathcal{U}_c . These strokes incorporate non-adiabatic driving protocols.

The generators of the isotherms can be derived from first principles under the following restrictions: (i) Weak system-bath coupling; (ii) Fast bath dynamics relative to the system and driving [36]; (iii) The protocol complies with the Inertial Theorem [37]. Specifically, for the parametric harmonic oscillator, Eq. (1), the inertial theorem is satisfied in the limit of a slow change in the adiabatic parameter, $d\mu/dt \rightarrow 0$, where $\mu = \dot{\omega}/\omega^2$. The adiabatic parameter can be large, indicating fast driving relative to the Bohr frequencies, while varying slowly. The resulting master equation is consistent with the thermodynamic laws [36, 43].

The Carnot analog cycle is constructed by concatenating four strokes:

- An expansion stroke (Fig. 1 Panel (a) corners $1 \rightarrow 2$), decreasing the oscillator frequency. while the system is coupled to a hot bath of a temperature T_h . This stroke is termed *open-expansion*, referring to the fact that during this segment the working medium is an open quantum system, exchanging energy and entropy with the bath. The evolution of the WM is governed by the propagator \mathcal{U}_h .
- *Adiabatic expansion* stroke ($2 \rightarrow 3$) in which the system is isolated from the baths and the oscillator frequency is decreased. The stroke is associated with the propagator \mathcal{U}_{ch} .
- *Open-compression* ($3 \rightarrow 4$), the particle is brought in contact with the cold bath of temperature T_c and 'compressed' towards a higher frequency, associated with the propagator \mathcal{U}_c .
- *Adiabatic compression* ($4 \rightarrow 1$), the final stroke restores the system to its initial state while keeping the particle isolated from the baths. The stroke propagator is \mathcal{U}_{hc} .

Formally, the complete cycle propagator can be decomposed to stroke propagators:

$$\mathcal{U}_{cyc} = \mathcal{U}_{hc}\mathcal{U}_c\mathcal{U}_{ch}\mathcal{U}_h \quad , \quad (3)$$

Each propagator \mathcal{U}_i is a completely positive map, associated with the cycle stroke. For a closed Lie algebra, the system dynamics can be described within a restricted operator vector space. Within this framework, we can represent the state as a generalized Gibbs form, which is the maximum entropy state under the constraint imposed by the observables of the Lie algebra [44, 45, 46]. The generalized Gibbs structure is preserved under the full dynamics of the cycle, this property is termed canonical invariance [47, 13, 36]. For the analysis, we choose operators motivated by thermodynamical insight: The instantaneous Hamiltonian and two additional operators to represent coherence the Lagrangian $\hat{L}(t)$ and $\hat{C}(t)$ (Cf. Appendix D). These operators do not commute with $\hat{H}(t)$, together they define the coherence measure [24]:

$$Coh = \frac{\sqrt{\langle \hat{L}(t) \rangle^2 + \langle \hat{C}(t) \rangle^2}}{\hbar\omega(t)} \quad . \quad (4)$$

Repeated operation of the cycle propagator, Eq. (3), converges to a unique limit cycle [48]. The thermodynamic analysis is then carried out on the limit cycle in terms of work W and heat Q . External work performed on the WM is defined in terms of the instantaneous power, $\text{tr}(\dot{\hat{H}}\hat{\rho})$, [8]

$$W = \int_0^t \langle \frac{\partial \hat{H}(t')}{\partial t'} \rangle dt' \quad , \quad (5)$$

and heat is obtained from the first law of thermodynamics $E = W + Q$.

3. Carnot-shortcut cycle

The Carnot-shortcut cycle is characterized by the four corners of the ideal Carnot cycle. Utilizing shortcut protocols, the WM transitions between the thermal states associated with the cycle corners in finite time. Starting from a thermal state the non-adiabatic protocols induce coherence generation and excitations leading to a non-equilibrium state. Generated coherence is then transferred to energy at the end of the stroke leading to the desired thermal state. In the long cycle time limit, the state follows the adiabatic change in the Hamiltonian and the cycle converges to the reversible Carnot cycle.

The switching points between strokes are defined in terms of the bath temperatures T_c, T_h and oscillator frequencies $\omega_1, \omega_2, \omega_3$ and ω_4 . Defining the compression ratio $\mathcal{C} = \omega_{max}/\omega_{min} = \omega_1/\omega_3$, the cycle is completely determined by $\omega_{min} = \omega_3$, \mathcal{C} and bath temperatures.

At the four corners the WM is in a thermal state: $\hat{\rho}_{th}(\omega, T) \equiv Z^{-1} \exp(-\hat{H}(\omega)/k_B T)$, where Z is the partition function (see Fig. 1 Panel (a)). The adiabatic strokes conserve the working medium's entropy. Therefore, the populations

satisfy $n_2 = 1/\left(\exp\left(\frac{\hbar\omega_2}{k_B T_h}\right) - 1\right) = n_3 = 1/\left(\exp\left(\frac{\hbar\omega_3}{k_B T_c}\right) - 1\right)$ and $n_1 = n_4$, where n_i is the population at the i 'th corner. This leads to the condition

$$\frac{\omega_3}{\omega_2} = \frac{\omega_4}{\omega_1} = \frac{T_c}{T_h} . \quad (6)$$

From the cycle definition $\omega_1 > \omega_2$ and using Eq. (6) we obtain a lower bound for the compression ratio

$$\mathcal{C} > \frac{T_h}{T_c} . \quad (7)$$

The Carnot-shortcut obtains non-vanishing power by utilizing Shortcut To Equilibration (STE) protocols [13] during the open-expansion and open-compression strokes (see Appendix A), and Shortcuts To Adiabaticity (STA) protocols for the adiabatic expansion and compression (see Appendix B).

Shortcut to equilibrium protocols are designed to manipulate an open quantum system between thermal states. The construction of these protocols is based on the inertial theorem [37] and the NAME [36]. Starting from a stationary Gibbs state the driving is first accelerated (complying with the inertial theorem) and then decelerated, leading to the target Gibbs state at the end of the stroke. In the present open-expansion process we modify the frequency from ω_1 to ω_2 while the system interacts with a bath at temperature T_h (or in the open-compression from ω_3 to ω_4 at bath temperature T_c). This protocol balances coherence generation and dissipation to achieve a Gibbs state, diagonal in the energy representation.

The protocol duration can be varied within the framework of the inertial approximation with negligible deviations from optimal fidelity [13]. Once the protocol duration is cut short, the STE requires a rapid change of the Hamiltonian, generating more intermediate coherence. This leads to larger dissipation, resulting in an increase of the entropy production and work cost.

On the adiabats, frictionless protocols are constructed employing the Lewis-Riesenfeld invariant [49, 12, 50]. These protocols vary the oscillator frequency non-adiabatically, generating coherence at intermediate times and storing energy in the WM. At the end of the stroke, the coherence is fully extracted, leading to a total zero work cost. Since all stored energy is retrieved when the protocol is completed, we consider these processes as an analog to catalysis [24]. In principle, these protocols can be achieved almost instantaneously. However, this implies a temporary storage of an infinite amount of energy in the WM [12, 50, 51]. To comply with practical physical considerations, we choose a constant stroke duration for the adiabats, which is consistent with the inertial theorem. Moreover, the cycle-time is dominated by the open-strokes, therefore the time allocated to the adiabats does not alter the performance qualitatively. A more complete description accounts for the power dissipated in the controller [52, 53], this contribution is out of the scope of the present analysis.

Control of the cycle time allows a transition between two extreme operation modes. Short cycle times produces finite power $\mathcal{P} = -W/\tau_{cycle}$, on account of a reduction in efficiency, due to quantum friction associated with fast driving. The non-adiabatic

driving generates coherence, which is dissipated to the bath. As a result, the useful work decreases, leading to a decrease in efficiency. In contrast, the long cycle time regime optimizes the efficiency while leading to a vanishing power output. Such cycle performance demonstrates the trade-off between power and efficiency.

Correspondence between the Carnot-shortcut cycle and the ideal classical result is obtained in the quantum adiabatic limit (diverging stroke times). In this limit, the WM state remains on the energy shell along the whole cycle and the STE and STA strokes converge to reversible isothermals and adiabats. The optimal work extraction becomes

$$W_C = \hbar\Delta\omega_{32}(n_2 + 1) + \hbar\Delta\omega_{14}(n_1 + 1) + k_B(T_h - T_c) \ln\left(\frac{n_1}{n_2}\right) , \quad (8)$$

where $\Delta\omega_{ij} = \omega_i - \omega_j$. In the high temperature limit Eq. (8) obtains the elegant form

$$W_C = -k_B T_h \eta_C \ln(\mathcal{C}) . \quad (9)$$

3.1. Performance of the Carnot-shortcut cycle

The performance of the Carnot-shortcut cycle is analysed by varying the duration of the open strokes, while keeping the time allocation of the adiabatic strokes fixed. We find two characteristic operational modes: Engine and dissipator. These are associated with different driving speed regimes. For ‘slow’ to ‘moderate’ driving speeds (‘long’ or ‘medium’ cycle-times) the cycle operates as an engine (negative work output and positive efficiency, using the convention that outgoing energy is negative). For decreasing cycle-times the work output of the *open-expansion* decreases (in absolute value) and the work required to perform the *open-compression* stroke increases. This leads to a reduced efficiency, see Fig. 2 Panel (a). Once the cycle-time is reduced below $\tau_{trans} = 23.87 (2\pi/\omega_{min})$, where $\omega_{min} = 5$ a.u, the cycle operates as a dissipator, converting net positive work to heat, which is in turn dissipated to the cold bath. This leads to negative efficiency for $\tau_{cycle} < \tau_{trans}$, as shown in Fig. 2 Panel (a).

The transition between dissipator and engine operational modes is caused by the large energy dissipation, which accompanies fast driving. Fig. 1 displays a map of the cycle in the energy frequency plane. For slow driving, Panel (a), the open-strokes follow the isotherms, leading to a Carnot-analog engine that obtains close to optimal efficiency $\eta_C = 0.375$. When the cycle-time shortens, the energy deviates significantly from the isotherms, Panel (b), and the cycle operates as a dissipator. Decrease in efficiency is attributed to fast driving, that requires large generation of coherence. Consequently, dissipation is increased, eventually canceling the useful extracted work. Geometrically, the reduction in work can be witnessed as a reduction in the area confined by the cycle, in the $\langle \hat{H} \rangle, \omega$ plane.

Since the adiabats are preformed by frictionless protocols, the cycle’s operational mode is dictated by the open strokes. In these strokes, decreasing the stroke times costs work, eventually damaging the performance. Such an effect is naturally described in the simplified asymptotic large cycle time limit. Asymptotically, the work cost scales as

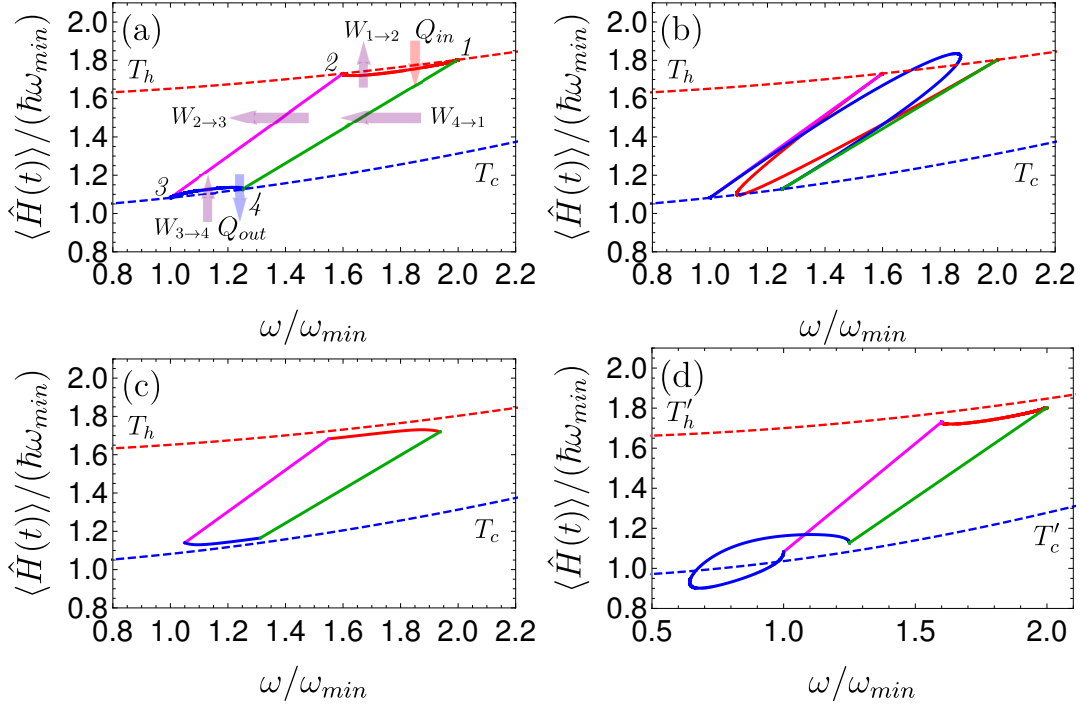


Figure 1. A map the Carnot-analog cycles: Energy as a function of the oscillator frequency ω . The Carnot-shortcut cycle for cycle-times: (a) $\tau_{cycle} = 250$, (b) $\tau_{cycle} = 17.5$, the (c) Endo-global cycle and (d) Endo-shortcut cycle for $\tau_{cycle} = 250$ (units of $2\pi/\omega_{min}$). Hot (red) and cold (blue) isotherms are indicated by dashed lines, in panel (d) the isotherms are displaced relative to the previous panels. Cycle strokes are color coded by: *open-expansion*-red, *adiabatic expansion*-purple, *open-compression*-blue and *adiabatic compression*-green. Model parameters are presented in table 1

$1/t$ [13] and the power behaves as, (Cf. Appendix C)

$$\mathcal{P} - \frac{|W_C|}{\tau_{cycle}} \propto -\frac{F}{\tau_{cycle}^2}, \quad (10)$$

where W_C is the ideal work, Eq. (8), and F is the friction action (see Appendix C). The three terms of Eq. (10) are positive for an engine operation, inferring that there exists a maximum in power for a finite cycle-time τ_{cycle}^\ddagger . Furthermore, for sufficiently small τ_{cycle} Eq. (10) implies that the power output is negative and the cycle becomes a dissipator. This leads to the approximate relation between the cycle-time at maximum power τ^* and the transition time τ_{trans} : $\tau^* = 2\tau_{trans}$. Fig. 2 demonstrates this approximate relation. Overall, reducing the cycle-time increases the invested work during the *open-compression* stroke, and reduces the work output in the *open-expansion*, in accordance with the thermodynamic principles.

For increased cycle-times, the efficiency of the cycle improves, obtaining the Carnot bound asymptotically (see Fig. 2 Panel (a)). Optimal power is achieved for relative short cycle-times $\tau_{max\mathcal{P}} = 43(2\pi/\omega_{min})$, (see Fig. 2 Panel (b)). We have also analyzed

\ddagger Eq. (10) can be written as a second order polynomial in the parameter $x = 1/\tau_{cycle}$, with $d^2\mathcal{P}/dx^2 < 0$.

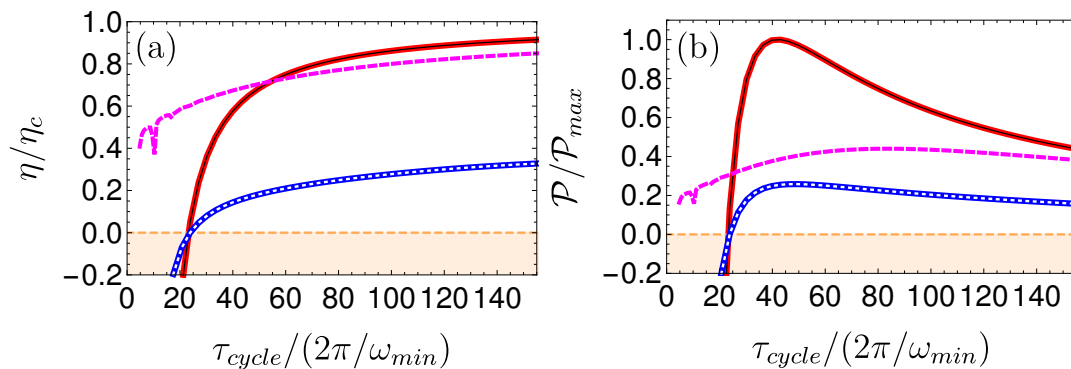


Figure 2. (a) Efficiency and (b) power as a function of cycle-time τ_{cycle} . The light orange background indicates negative output power; a dissipator. Here, $\eta_C = 0.375$, $\mathcal{P}_{max} = 6.3 \cdot 10^{-3}$ a.u. When $\tau_{cycle} > \tau_{trans}$ the Carnot-analog cycle operates as an engine, for $\tau_{cycle} < \tau_{trans}$ the cycle operates as a dissipator.

the performance at elevated temperatures, maintaining a constant temperature ratio. Asymptotically, the power increased linearly, Eq. (9), and the efficiency at maximum power converged to the value $\eta_{max\mathcal{P}}^*$ slightly larger than η_{CA} . This implies that this cycle does not operate in the weak dissipation limit [7].

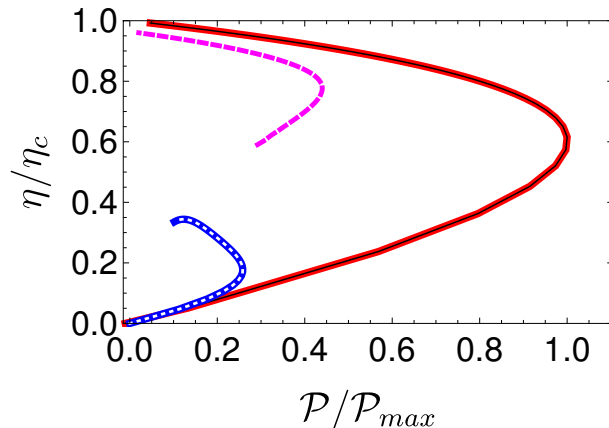


Figure 3. Normalized efficiency as a function of the normalized power for the Carnot-shortcut (red, with thin black line), Endo-global (thin dashed magenta) and Endo-shortcut (blue with white dots) cycles. The Carnot efficiency is $\eta_C = 0.375$, and the value of the efficiency at maximum power $\eta_{max\mathcal{P}} = 0.62\eta_C$ slightly greater than the Curzon-Ahlborn efficiency $\eta_{CA} = 0.56\eta_C$.

4. Quantum signature: Endoreversible Shortcut and Global Carnot cycles

Endoreversible cycles are defined by four corners for which the WM is in a Gibbs state with temperatures $T \neq T'_{bath}$. As a result, finite heat flow between the engine and bath occurs and the WM is never in equilibrium with the heat bath. In the following, primes designate the bath temperatures of the endoreversible cycle.

The Endo-shortcut cycle is constructed in a similar fashion to the Carnot-shortcut cycle Sec. 3, including two STE and two STA protocols. For such a cycle, the STE protocols are modified to transform the state between non-equilibrium Gibbs states, Cf. Appendix A.1. As a result, the four corners are maintained in a non-equilibrium Gibbs state $\hat{\rho}(\omega, T) = Z^{-1} \exp(-\hat{H}(\omega)/k_B T)$, keeping the same frequencies $(\omega_1 - \omega_4)$, where T is the working medium's internal temperature which differs from the bath temperatures T'_c and T'_h . The bath temperatures of the Endo-shortcut cycle satisfy $T'_c < T_c$ and $T'_h > T_h$, relative to the Carnot-shortcut bath temperatures T_c and T_h , see Table 1 for a summary of the various cycle parameters. During the open-expansion the STE transfers the oscillator from $\hat{\rho}(\omega_1, T_h)$ to $\hat{\rho}(\omega_2, T_h)$, and similarly in the open-compression ($\omega_4 \rightarrow \omega_1$ with $T = T_c$), see Fig. 1 Panel (d).

Alternatively, the *Endo-global* cycle operates as a Carnot-analog cycle where the strokes are performed with a pre-defined constant adiabatic speed $|\mu| = |\dot{\omega}/\omega^2| = \text{const.}$ The strokes are defined by four frequencies $\omega_1^g, \omega_2^g, \omega_3^g, \omega_4^g$, and μ . These determine the stroke duration t_f and protocols $\omega(t) = \omega_i/(1 - \mu\omega_i t)$ for a stroke starting at ω_i and ending at $\omega(t_f)$, Cf. Appendix D.

Propagators of the free dynamics, Eq. (1), can be obtained explicitly in terms of an operator basis in Liouville space Cf. Appendix D. These propagators construct the WM unitary transformations of the adiabats. Next, the same free dynamics solution is used to derive the NAME, employed to generate the propagator of the *open-expansion*, \mathcal{U}_h , and *open-compression*, \mathcal{U}_c , strokes [36]. Combining the four strokes forms the Global cycle.

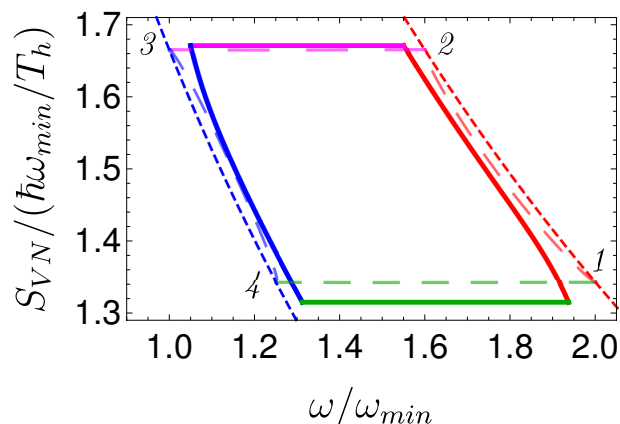


Figure 4. Cycle map: von Neumann Entropy $S_{v,n}$ as a function of the oscillator frequency $\omega(t)$ for the Endo-global cycle (thick continuous lines) and Carnot-shortcut cycle (transparent long dashed), in the slow driving regime $\tau_{cycle} = 250(2\pi/\omega_{min})$. The Endoreversible cycle operates between the hot (short-dashed red) and cold (short-dashed blue) isotherm lines of temperatures $T_h = 8$ and $T_c = 5$.

In the following, we analyze an Endo-global Carnot cycle operating between baths of temperatures T_c and T_h , with frequencies $\omega_1^g = T_h^g(\omega_1/T_h)$, $\omega_3^g = T_c^g(\omega_3/T_c)$, $\omega_2^g = \omega_3^g(T_h^g/T_c^g)$ and $\omega_4 = \omega_1^g(T_c^g/T_h^g)$, where $T_c^g = 5.25$ and $T_h^g = 7.75$. The

frequencies are chosen so as to comply with an ideal Carnot cycle (or Carnot-shortcut cycle) operating between temperatures T_c^g and T_h^g , in the long cycle-time limit. In this limit, the state at the four corners becomes isoentropic with the states of the Carnot-shortcut cycle. As a result, the power of the two cycles coalesce at long cycle times, see Fig. 2 Panel (b). Thermodynamic analysis is carried out on the limit-cycle [48], defined by the cycle parameters above.

4.1. Cycle performance comparison

Performance of the three cycles is compared with an emphasis on the role of coherence. The cycle output is determined by the operational mode and the cycle parameters: Cycle frequencies, bath temperatures and cycle-time, Cf. Table 1. The Shortcut cycles (Carnot and endoreversible) are characterized by a branch coherence operation, where coherence is created ‘locally’ during each stroke, with initial and final diagonal Gibbs states. This can be seen in Fig. 5, where the dashed lines represent the coherence of the Carnot shortcut cycle which vanish after each stroke. Conversely, in the limit-cycle of the Endo-global engine, coherence is maintained throughout the cycle (globally) (non-vanishing continuous line in Fig. 5). As a result, coherence generated in one stroke can be utilized along the subsequent strokes.

This comparison is unbiased, since the same bath temperatures are considered for the Carnot-shortcut and Endo-global cycles. In the Endo-shortcut cycle, despite of the larger temperature difference there is no foreseen advantage.

The Carnot-shortcut cycle shows a superior performance at moderate and long cycle-times, Figs. 2 and 3. In this operational regime, the efficiency, power, maximum power, and efficiency at maximum power exceed both the Endo-global and Endo-shortcut cycles. However, for short cycle-times, both shortcut cycles become dissipators, producing negative power, while the Endo-global cycle continues to operate as an engine.

This behaviour compels us to reexamine the question: When is a quantum heat engine quantum? An intuitive approach defining a quantum signature, is that by observing the engine operation it will cease to produce useful output. To be more precise we can imagine continuously monitoring the energy of the WM on the adiabatic strokes. As a result, the state will relax to a diagonal state in the energy representation and coherence vanishes. The back action of the weak measurement is therefore equivalent to pure dephasing [54, 55], described by the master equation:

$$\frac{d}{dt}\hat{\rho}(t) = -\frac{i}{\hbar} \left[\hat{H}(t), \hat{\rho}(t) \right] - \gamma_d \left[\hat{H}(t), \left[\hat{H}(t), \hat{\rho}(t) \right] \right] , \quad (11)$$

where the parameter γ_d scales the dephasing rate. The explicit derivation is found in Appendix F. The influence of the dephasing rate on the engine efficiency is shown in Fig. 6. For long cycle-times where the nonadiabatic effects are small the influence of dephasing is minor. Conversely, for short cycle-times the engine operation requires coherence and the strong dephasing nulls the power output. Similar behaviour has been observed in the sudden Otto cycle and the two-stroke NV engines [24, 56, 39].

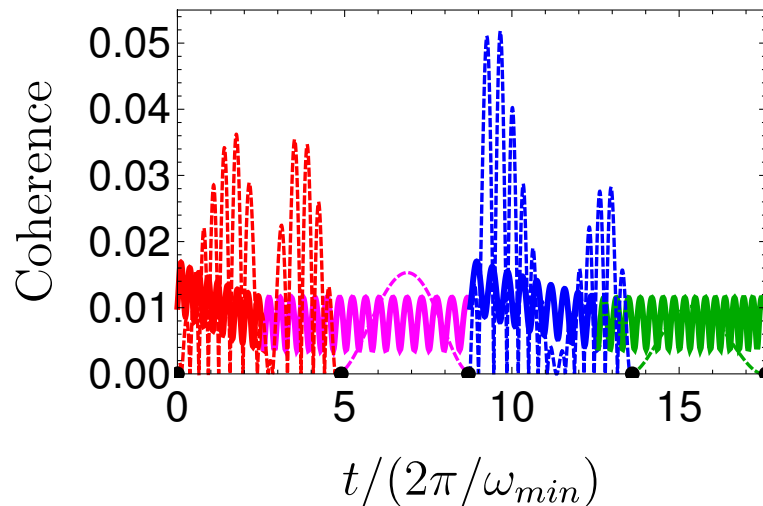


Figure 5. Coherence as a function of time for the Endo-global (continuous lines) and Carnot-shortcut (dashed lines) engines for a complete cycle with cycle-time $\tau_{cycle} = 8$ (units of $2\pi/\omega_{min}$). Cycle strokes are color coded as in Fig. 1. Endo-global engine is characterized by a global coherence operation, maintaining a non-vanishing coherence throughout the whole cycle. In contrast, the Carnot-shortcut exhibits branch coherence operation, coherence is created ‘locally’ during each stroke, with initial and final diagonal Gibbs states. Note, that the coherence of the Carnot-shortcut cycle vanishes at the intersections between adjacent strokes. The Endo-shortcut shows a similar behaviour as the Carnot-shortcut, it has been removed for clarity.

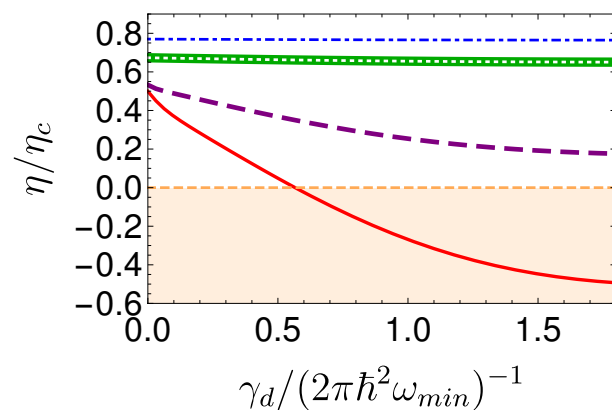


Figure 6. Normalized efficiency as a function of the dephasing strength γ_d , for $\tau_{cycle} = 8$ (red continuous line), $\tau_{cycle} = 12$ (purple-dashed), $\tau_{cycle} = 40$ (thick green with white dots), and $\tau_{cycle} = 80$ (blue-dot-dashed) (units of $2\pi/\omega_{min}$). For short cycle-times, coherence becomes central to the engine’s operation. In this regime, increasing the dephasing strength leads to a reduction of efficiency. On the other hand, when the driving is slow, generation of coherence is small and the dephasing does not affect the engine’s performance. Note, that for negative efficiency the cycle operates as a dissipator.

Another viewpoint on quantum signatures arises from a comparison with the classical counterpart. Introducing strong dephasing effectively leads to a pure stochastic mode of operation, where the system is solely characterized by its population in the

Table 1. Cycle parameters

| Cycle type | Carnot-shortcut | Endo-Shortcut | Endo-global |
|--------------------|--|--|---|
| Baths temperatures | $T_c = 5$ $T_h = 8$ | $T'_c = 5.25$ $T'_h = 7.75$ | $T_c = 5$ $T_h = 8$ |
| Cycle frequencies | $\omega_1 = 10$ $\omega_2 = \omega_3 \frac{T_h}{T_c} = 6.25$ $\omega_3 = 5$ $\omega_4 = \omega_1 \frac{T_c}{T_h} = 7.5$ | $\omega_1 = 10$ $\omega_2 = 6.25$ $\omega_3 = 5$ $\omega_4 = 7.5$ | $\omega_1^g = 9.6875$ $\omega_2^g = 7.75$ $\omega_3^g = 5.25$ $\omega_4^g = 6.5625$ |
| Operation type | Branch coherence | Branch coherence | Global coherence |

energy representation and the energy levels. The improved efficiency, in the small cycle time regime, demonstrates that for fast driving the coherent operation mode outperforms the stochastic work extraction mechanism. This highlights the quantum advantage in this regime. The relative increase of efficiency under coherent operation also constitutes a thermodynamic measurable quantity that indicates the existence of a pure quantum phenomena. Therefore, it is considered as a quantum signature. In essence, coherence emerges when the WM state is in a superposition of eigenstates of the instantaneous Hamiltonian, implying that the superposition nature is the origin of the increased efficiency and quantum signature.

4.2. Geometric representation of coherence

To illuminate the interplay between coherence and energy throughout the Carnot analog cycles, we present a geometrical representation of the WM state. Generally, a Gaussian state of the Harmonic oscillator is fully characterized by a basis of four operators forming a closed Lie algebra. Moreover, assuming an initial Gaussian form, the WM state is canonical invariant under the equations of motion of the various strokes [47, 24]. We chose a time-dependent operators basis $\{\hat{H}(t), \hat{L}(t), \hat{C}(t)\}$, see Sec. 2 and Appendix D. This leads to the geometrical representation in terms of the vector $\vec{v}(t) = \{\langle \hat{H} \rangle, \langle \hat{L} \rangle, \langle \hat{C} \rangle\}^T$, shown in Figure 7.

Coherence in the energy basis is related to the operators $\hat{L}(t)$ and $\hat{C}(t)$ which do not commute with $\hat{H}(t)$, Appendix D Eq. (D.1). The shortcut cycles, shown in Panels (a) and (b) display significant coherence generation, with an overshoot in energy during the open-strokes. The Lewis-Riesenfeld protocols of the adiabatic strokes lead to $\langle \hat{L}(t) \rangle \approx 0$ [50]. In this cycle, all the connecting corners between strokes are on the line $\langle \hat{L} \rangle = \langle \hat{C} \rangle = 0$. The trajectory of the Endo-global cycle encircles the zero coherence line $\langle \hat{L} \rangle = \langle \hat{C} \rangle = 0$, while never coinciding with it. As expected, short cycle-times lead to greater coherence, Panel (c).

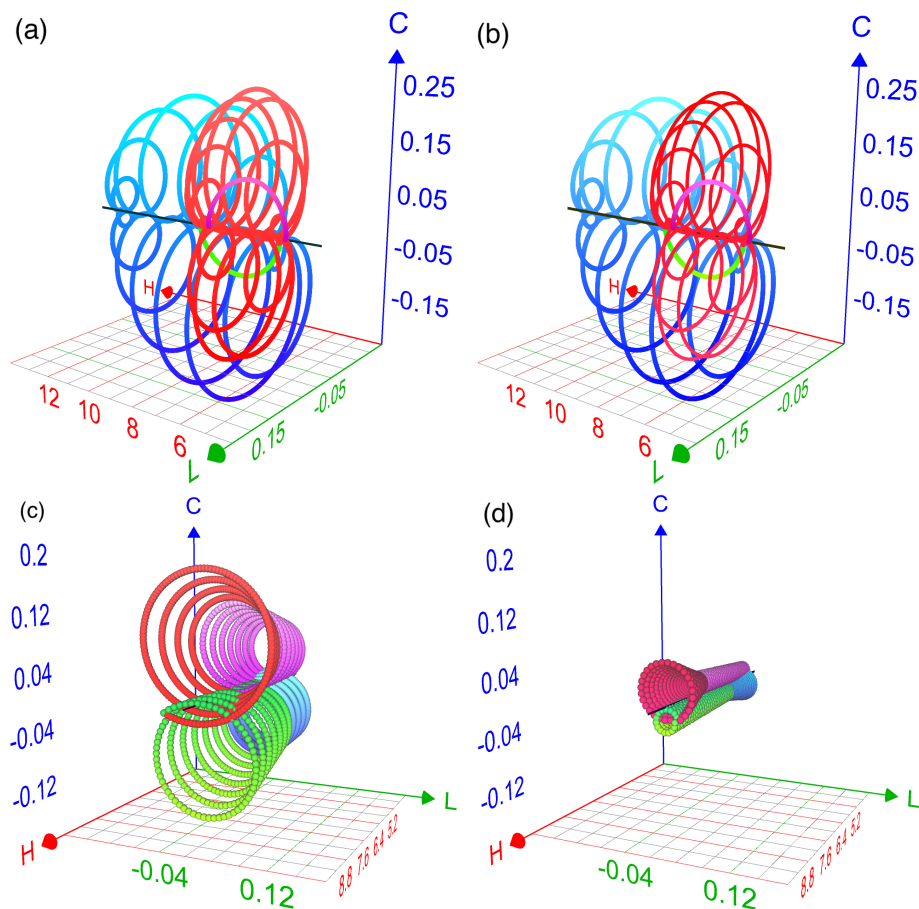


Figure 7. Cycle trajectory in the $\{\langle\hat{H}\rangle, \langle\hat{L}\rangle, \langle\hat{C}\rangle\}$ observable vector space, where \hat{L} is the Lagrangian, \hat{C} is the position momentum correlation operator and \hat{H} is the Hamiltonian Eq. (1) [24]. The red and blue lines display the open-expansion and compression strokes and the purple and green lines display the expansion and compression unitary strokes. Panel (a) shows the Shortcut cycle (b) Endo-shortcut cycle for a fast driving $\tau_{cycle} = 17.5$ (c),(d) Endo-global cycle for $\tau_{cycle} = 8$ and $\tau_{cycle} = 32$ (units of $2\pi/\omega_{min}$). The black line designates zero coherence $\langle\hat{L}\rangle = \langle\hat{C}\rangle = 0$. Note, that in the shortcut trajectories coherence vanishes at the cycle's four corners.

5. Discussion

A family of finite power quantum Carnot-analog engines is investigated to determine the role of coherence in the engine operation. In the construction of the models, we have overcome the difficulty of describing thermalization in the presence of non-adiabatic driving [36], including an explicit description of the working medium dynamics. This enables a comparison to other finite-time quantum cycle as the Otto cycle [24].

Carnot and Otto engines have been the keystones in the study of quantum heat devices. These engines differ by their thermalization strokes and share their unitary adiabatic strokes. For a fair comparison, we assume the same working medium and bath temperatures. The Otto and Carnot cycles have different permissible compression ratio range. The Otto cycle is constrained by $\frac{T_h}{T_c} \geq C > 1$, while the compression ratio

of the Carnot cycle obeys $\mathcal{C} > \frac{T_h}{T_c}$. Optimal work for the Otto cycle is achieved when $\mathcal{C} = \sqrt{\frac{T_h}{T_c}}$ and vanishes in limits $\mathcal{C} = 1$ and $\mathcal{C} = \frac{T_h}{T_c}$. On the other hand, the power of the Carnot-analog has a local optimum, and the work output diverges with \mathcal{C} , Eq. (9).

A major performance measure of engines is the efficiency. Otto and the Carnot cycles have different efficiency characteristics, in particular, their dependence on the compression ratio and bath temperatures. The Otto efficiency $\eta_O = 1 - \mathcal{C}^{-1}$ converges to η_C in the limit of zero work. Moreover, optimal efficiency increases conjointly with the work, achieving $\eta_O = \eta_{CA}$ at the optimum power point in the high temperature limit [47]. Conversely, for the Carnot-shortcut cycle, efficiency η_C is constant as function of compression ratio, while the work monotonically increases with \mathcal{C} . For this cycle the power obtains its optimum at a finite compression ratio. In addition, the efficiency at maximum power is found to be greater than the Curzon-Ahlborn efficiency $\eta_{maxP} > \eta_{CA}$.

Control of coherence is the key to obtain finite-power in quantum engines. Shortcut protocols utilize coherence temporally to accelerate the dynamics and enhance the power. On the adiabatic unitary strokes, shortcuts (STA) can be obtained with no direct cost, Sec. 2 [28, 29]. For the thermalization strokes, STE protocols enable swift equilibration. This is achieved by generating significant coherence which increases the dissipation of energy and information to the bath. As a result, such a speedup is accompanied by an additional work cost. These protocols are incorporated in the operation of the Carnot-shortcut and Endo-shortcut. The dissipated potential work in the cycle explains the mechanism leading to the power-efficiency tradeoff, and the existence of a minimum cycle time [47, 57, 58, 59]. Similar STE protocols can also be used to accelerate the thermalization in the Otto and Stirling cycle. In addition, STE protocols can be experimentally realized in engines with harmonic working fluid as well as a spin system [17, 18, 60].

The Endo-global cycle is characterized by non-vanishing coherence throughout the cycle operation, Fig. 5. This is in contrast to the shortcut cycles, which are diagonal in energy representation at the four corners of the cycle. Global coherence enables engine operation at short cycle-times, where the Endo-Shortcut and Carnot-Shortcut become dissipators. This indicates a quantum signature[39]. In the presence of pure-dephasing, the coherence vanishes, reducing power and efficiency. Eventually, strong dephasing transforms the cycle from an engine to a dissipator, a signature of a pure quantum operational mode, see Fig. 6.

To conclude, the motto of this study follows Carnot's tradition of learning by example. The analysis of a solvable cycle has unraveled the role of coherence. On one hand, coherence is responsible for quantum friction, and on the other hand it allows rapid thermalization and a coherent mode of operation.

Acknowledgments

We thank Peter Salamon for inspiring this study. We also gratefully acknowledge KITP for their hospitality, and the support of the Adams Fellowship Program of

the Israel Academy of Sciences and Humanities. Partial funding was supplied by the National Science Foundation under Grant No. NSF PHY-1748958 and the Israel Science Foundation Grant No. 2244/14.

Appendix A. Shortcut to equilibration protocol

The STE protocol rapidly transfers the working medium between two Gibbs states with different entropies. Construction of the protocol relies on the Non-Adiabatic Master Equation (NAME) [36] and the Inertial Theorem [37]. Derived from first principles, the NAME describes the reduced dynamics of a non-adiabatically driven open quantum system in the weak coupling Markovian regime. The NAME incorporates, as a limit, both the adiabatic and periodic Floquet master equations.

The derivation of the NAME requires an explicit solution of the closed system dynamics. Utilizing the inertial theorem, we obtain the free propagator $\hat{U}_S(t)$ for slowly ‘accelerated’ external control. For this study, we considered a harmonic oscillator working medium, where the control is achieved by varying the potential. In this case, the inertial condition is associated with a slow change in the adiabatic parameter $\mu = \dot{\omega}/\omega^2$. The explicit solution of free dynamics propagator allows to transform the system-bath coupling to the interaction representation. Using the Born-Markov approximation we derive the generator of the open system dynamics. For this case, we consider an Ohmic Boson bath with Markovian properties. The derivation leads to the reduced system dynamics in the interaction representation

$$\begin{aligned} \frac{d}{dt}\tilde{\rho}_S(t) = \mathcal{L}\tilde{\rho} = & k_{\downarrow}(t) \left(\hat{b}\tilde{\rho}_S(t)\hat{b}^{\dagger} - \frac{1}{2}\{\hat{b}^{\dagger}\hat{b}, \tilde{\rho}_S(t)\} \right) \\ & + k_{\uparrow}(t) \left(\hat{b}^{\dagger}\tilde{\rho}_S(t)\hat{b} - \frac{1}{2}\{\hat{b}\hat{b}^{\dagger}, \tilde{\rho}_S(t)\} \right) . \end{aligned} \quad (\text{A.1})$$

Here, the density operator in the interaction picture reads $\tilde{\rho}_S(t) = \hat{U}_S(t, 0) \hat{\rho}_S(t) \hat{U}_S^{\dagger}(t, 0)$.

$$k_{\downarrow}(t) = k_{\uparrow}(t) e^{\alpha(t)/k_B T} = \frac{\alpha(t) |\vec{d}|^2}{4\pi\epsilon_0\kappa\hbar c} (1 + N(\alpha(t))) , \quad (\text{A.2})$$

where N is the occupation number of the Bose-Einstein distribution, $\kappa = \sqrt{4 - \mu^2}$, and α is a modified frequency, determined by the non-adiabatic driving protocol [36]. In terms of the oscillator frequency, the modified frequency is given by

$$\alpha(t) = \sqrt{1 - (\dot{\omega}(t)/(2\omega^2(t)))^2} \omega(t) . \quad (\text{A.3})$$

The Lindblad jump operators become $\hat{b} \equiv \hat{b} \equiv \hat{b}(0) = \sqrt{\frac{m\omega(0)}{\kappa\hbar} \frac{\kappa+i\mu}{2}} \left(\hat{Q}(0) + \frac{\mu+i\kappa}{2m\omega(0)} \hat{P}(0) \right)$.

In the adiabatic driving limit, $\mu \rightarrow 0$, the Lindblad jump operators converge to the adiabatic creation and annihilation operators $\hat{b}^{\dagger}, \hat{b} \rightarrow \hat{a}^{\dagger}, \hat{a}$. Therefore, in this limit, Eq. (A.1) reduces to the adiabatic master equation.

The completely positive map generated by Eq. (A.1) preserves the Gaussian form. This property is termed canonical invariance [44, 61, 47, 24]. Formally, the Gaussian state can also be expressed in a product form

$$\tilde{\rho}_S(t) = Z^{-1} e^{\gamma(t)\hat{b}^2} e^{\beta(t)\hat{b}^{\dagger}\hat{b}} e^{\gamma^*(t)\hat{b}^{\dagger 2}} , \quad (\text{A.4})$$

where $Z = \text{tr} \left(e^{\gamma(t)\hat{b}^2} e^{\beta(t)\hat{b}^\dagger\hat{b}} e^{\gamma^*(t)\hat{b}^{\dagger 2}} \right)$, the operators $\hat{b}^\dagger\hat{b}$, \hat{b}^2 , $\hat{b}^{\dagger 2}$ vary with μ . Parameters γ and β are time-dependent functions.

For an initial thermal state, the construction is simplified and the reduced system remains in the following form throughout the entire evolution

$$\tilde{\rho}_S(\beta(t), \mu(t)) = Z^{-1} e^{\beta\hat{b}^\dagger\hat{b}(\mu)} \quad , \quad (\text{A.5})$$

with initial conditions $\beta(0) = -\frac{\hbar\omega(0)}{k_B T}$ and $\mu(0) = 0$. Substituting Eq. (A.5) into Eq. (A.1) leads to a non-linear differential equation for $\beta(t)$

$$\dot{\beta} = k_\downarrow(t) (e^\beta - 1) + k_\uparrow(t) (e^{-\beta} - 1) \quad . \quad (\text{A.6})$$

Equation (A.6) constitutes the basis for the STE control scheme. We define $y(t) \equiv e^{\beta(t)}$ and guess a polynomial solution for y . This solution should transfer an initial thermal state of frequency $\omega(0)$ to a final thermal state with a frequency $\omega(t_f)$, which leads to the boundary conditions $\beta(0) = -\frac{\hbar\omega(0)}{k_B T}$, $\beta(t_f) = -\frac{\hbar\omega(t_f)}{k_B T}$ and $\mu(0) = \mu(t_f) = 0$. Furthermore, the condition on μ implies that the state and protocol are stationary at initial and final times, leading to $\dot{\beta}(0) = \dot{\beta}(t_f) = \ddot{\beta}(0) = \ddot{\beta}(t_f)$.

A fifth-degree polynomial is sufficient to comply with all the boundary conditions. The solution reads

$$y(s) = y(0) + c_3 (t/t_f)^3 + c_4 (t/t_f)^4 + c_5 (t/t_f)^5 \quad , \quad (\text{A.7})$$

where $c_3 - c_5$ are determined from the boundary conditions $y(0) = e^{\beta(0)}$, $y(t_f) = e^{\beta(t_f)}$, and $\dot{y}(0) = \dot{y}(t_f) = \ddot{y}(0) = \ddot{y}(t_f) = 0$. Next, we insert the solution for y , Eq. (A.7), into Eq. (A.6) and solve for $\alpha(t)$. The control $\omega(t)$ is obtained by solving Eq. (A.3) by numerical means.

Appendix A.1. STE for non-thermal initial and final states

The Endo-shortcut cycle, Sec. 4, includes *open-compression* and *open-expansion* strokes between non-equilibrium states. During these strokes, the working medium state is of the Gibbs form

$$\hat{\rho}(t) = Z^{-1} e^{-\frac{\hbar\omega(t)}{k_B T_i}} \quad , \quad (\text{A.8})$$

where the internal temperatures T_i and T_f differs from the bath temperatures, i.e., $T_i = T_f \equiv T_0 \neq T$.

The control protocol $\omega(t)$ for the open-strokes is obtained by a similar reverse-engineering method as in the case of an initial and final equilibrium states ($T_i, T_f = T$). However, since the system-bath interaction leads to non-vanishing decay rates, the initial and final states are non-stationary, which implies $\dot{\beta}(0), \dot{\beta}(t_f) \neq 0$. As in the previous construction, we require a continuous change in the control protocol, associated with the restriction $\dot{\omega}(0) = \dot{\omega}(t_f) = 0$. Substituting the condition $\dot{\omega}(0) = 0$ into the decay rates of Eq. (A.6) we obtain the initial value for $\dot{\beta}$ (this is in accordance with the dynamics of the time-independent master equation [62]). This leads to the boundary conditions for y : $y(0) = y(0) = \exp\left(-\frac{\hbar\omega(0)}{k_B T_0}\right)$, $\dot{y}(0) = \dot{\beta}(0) \exp\left(-\frac{\hbar\omega(0)}{k_B T_i}\right)$, $y(t_f) = \exp\left(-\frac{\hbar\omega(t_f)}{k_B T}\right)$,

$\dot{y}(t_f) = \dot{\beta}(t_f) \exp\left(-\frac{\hbar\omega(t_f)}{k_B T_0}\right)$ and $\ddot{y}(0) = \ddot{y}(t_f) = 0$. Following a similar derivation as the previous section, we introduce a fifth order polynomial that satisfies the boundary conditions to obtain $\omega(t)$.

Appendix B. Adiabatic strokes - Shortcut to adiabaticity protocols utilizing the Lewis Riesenfeld invariant

The (thermodynamic) adiabatic strokes are achieved utilizing shortcut to adiabaticity (STA) protocols. These transform a diagonal state in the energy basis, of a frequency ω_i , to a state with the same population, with a final frequency ω_f . These protocols are engineered utilizing the Lewis-Riesenfeld invariant [49]. We follow a similar procedure as presented in Refs. [49, 12] to construct the STA protocols.

We introduce an Hermitian invariant \hat{I} for the harmonic oscillator algebra, SU(1,1). Generally, such an invariant can be expressed as sum of the algebra operators

$$\hat{I}(t) = \frac{1}{2} \left(\alpha(t) \hat{Q}^2 + \beta(t) \hat{P}^2 + \gamma \left(\hat{Q}\hat{P} + \hat{P}\hat{Q} \right) \right) , \quad (\text{B.1})$$

and must satisfy the condition

$$\frac{d\hat{I}}{dt} = \frac{\partial \hat{I}}{\partial t} + \frac{1}{i\hbar} [\hat{I}, \hat{H}] = 0 . \quad (\text{B.2})$$

To obtain transition-less driving we desire a protocol for which the invariant commutes with the Hamiltonian at initial and final times:

$$\left[\hat{H}(0), \hat{I}(0) \right] = \left[\hat{H}(t_f), \hat{I}(t_f) \right] = 0 . \quad (\text{B.3})$$

Since the operators share a common eigenstate basis at these times and the eigenvalues of \hat{I} are stationary, the engineered protocol induces transition between two diagonal states in the energy representation.

Substituting Eq. (B.1) into Eq. (B.2) leads to three coupled differential equations for the time-dependent coefficients

$$\begin{aligned} \dot{\alpha} &= 2m\omega^2\gamma \\ \dot{\beta} &= -\frac{2}{m}\gamma \\ \dot{\gamma} &= -\frac{1}{m}\alpha + m\omega^2\beta \end{aligned} . \quad (\text{B.4})$$

By defining $\beta \equiv \sigma^2$ and conducting some algebraic manipulations (see Ref [49]) Eqs. (B.4) can be represented in terms of a single differential equation

$$\frac{d}{dt} (m^2\omega^2\sigma + m^2\ddot{\sigma}) \sigma + 3\dot{\sigma} (m^2\omega^2\sigma + m^2\ddot{\sigma}) = 0 . \quad (\text{B.5})$$

Solving for $m^2\omega^2\sigma + m^2\ddot{\sigma}$ and substituting the solution into Eq. (B.5) gives

$$\frac{c}{\sigma^2} = m^2\omega^2\sigma^2 + m^2\sigma\ddot{\sigma} , \quad (\text{B.6})$$

where, c is an arbitrary real integration constant. Next, we define $\sigma = c^{1/4}\rho$, and substitute the definition into Eq. (B.6), to obtain

$$\hat{I}(t) = \frac{1}{2} \left(\frac{1}{\rho^2} \hat{Q}^2 + \left(m\dot{\rho}\hat{Q} - \rho\hat{P} \right) \right) , \quad (\text{B.7})$$

with the subsidiary condition (Eq. (B.6))

$$m^2\omega^2(t)\rho + m^2\ddot{\rho} - \frac{1}{\rho^3} = 0 \quad . \quad (\text{B.8})$$

This equation introduces constraints on the protocol $\omega(t)$, which comply with the boundary conditions of $\rho(t)$. The strategy to engineer a transition-less control protocol is to choose $\rho(t)$ such that relations Eq. (B.3) are satisfied. This leads to the following boundary conditions

$$\begin{aligned} \dot{\rho}(0) &= \ddot{\rho}(0) = \dot{\rho}(t_f) = \ddot{\rho}(t_f) = 0 \\ \rho(0) &= \frac{1}{\sqrt{m\omega(0)}} \\ \rho(t_f) &= \frac{1}{\sqrt{m\omega(0)}} \sqrt{\frac{\omega_0}{\omega_f}} \quad . \end{aligned} \quad (\text{B.9})$$

Equation (B.8) is now solved by introducing a polynomial solution. A fifth order polynomial in t is sufficient to satisfy the conditions of Eq. (B.9). We substitute the polynomial solution into Eq. (B.8) and solve for $\omega(t)$.

To obtain the expectation values of \hat{H} , \hat{L} and \hat{C} , we introduce the eigenstates of $\hat{I}(t)$. These obey the eigenvalue equation

$$\hat{I}(t) |\lambda(t)\rangle = \lambda |\lambda(t)\rangle \quad , \quad (\text{B.10})$$

with time-dependent eigenstates and time-independent eigenvalues λ . Next, we define the annihilation operator $\hat{c} = 2\hbar^{-1} \left(\hat{Q}/\rho - i \left(m\dot{\rho}\hat{Q} - \rho\hat{P} \right) \right)$ and matching annihilation operator. These operators satisfy: $\hat{c}|\lambda\rangle = \sqrt{\lambda}|\lambda-1\rangle$ and $\hat{c}^\dagger|\lambda\rangle = \sqrt{\lambda+1}|\lambda+1\rangle$. By expressing \hat{H} , \hat{L} and \hat{C} in terms of \hat{c} and \hat{c}^\dagger one obtains

$$\begin{aligned} \langle\lambda|\hat{H}|\lambda\rangle &= \frac{\hbar}{2} \left(m\dot{\rho}^2 + \frac{1}{m\rho^2} + m\omega^2(t)\rho^2 \right) \left(\lambda + \frac{1}{2} \right) \\ \langle\lambda|\hat{L}|\lambda\rangle &= \frac{\hbar}{2} \left(m\dot{\rho}^2 + \frac{1}{m\rho^2} - m\omega^2(t)\rho^2 \right) \left(\lambda + \frac{1}{2} \right) \\ \langle\lambda|\hat{C}|\lambda\rangle &= \omega(t) \hbar m \dot{\rho} \rho \left(\lambda + \frac{1}{2} \right) \quad . \end{aligned} \quad (\text{B.11})$$

The final step is to sum over the contribution of each state $|\lambda\rangle$. For an initial Gibbs state the energy reads

$$\begin{aligned} \langle\hat{H}\rangle &= \text{tr} \left(\hat{\rho}\hat{H} \right) = \sum_{\lambda,\lambda'} \langle\lambda|\hat{\rho}|\lambda'\rangle \langle\lambda'|\hat{H}|\lambda\rangle \\ &= \sum_{\lambda} \langle\lambda|\hat{\rho}|\lambda\rangle \langle\lambda|\hat{H}|\lambda\rangle \\ &= \sum_{\lambda} \frac{e^{-\hbar\omega(0)(\lambda+\frac{1}{2})/k_B T}}{\mathcal{Z}} \langle\lambda|\hat{H}|\lambda\rangle \\ &= \frac{1}{2} \left(m\dot{\rho}^2 + \frac{1}{m\rho^2} + m\omega^2(t)\rho^2 \right) \frac{1}{2} \coth \left(\frac{\hbar\omega(0)}{2k_B T} \right) \quad . \end{aligned} \quad (\text{B.12})$$

The derivation for $\langle\hat{L}\rangle$ and $\langle\hat{C}\rangle$ follows a similar procedure.

Appendix C. Friction action

Shortcut to equilibrium processes rely on non-adiabatic driving of an open quantum system. The driving incorporates the dissipative and unitary dynamics to lead the system towards a target thermal state. These protocols accelerate the system thermalization rate by generating coherence at intermediate times (transforming energy

to coherence), and terminating them at the end of the protocol. The protocol duration τ_{stroke} of the STE can be varied within the inertial approximation, with a negligible influence on the final fidelity. For increasing protocol duration, the generation of coherence reduces, converging to the quantum-adiabatic result in the limit $\tau_{stroke} \rightarrow \infty$. As a result, as the protocol duration increases less coherence dissipates to the bath and the work output improves (reduced in the convention of $W < 0$ for work extraction). Asymptotically, the work output scales as τ_{stroke}^{-1} [13], therefore, one can introduce the ‘friction action’ F and express the total cycle work output W as a function of the ideal work W_C and F

$$W = W_C + \frac{F}{\tau_{cycle}} . \quad (\text{C.1})$$

In the quantum adiabatic limit the process is optimal and the work output converges to W_C , Eq. (8). Substituting Eq. (C.1) into the expression for the power output $\mathcal{P} = -W/\tau_{cycle}$, leads to the asymptotic relation

$$\mathcal{P} - \frac{|W_C|}{\tau_{cycle}} \propto -\frac{F}{\tau_{cycle}^2} . \quad (\text{C.2})$$

Equation (C.2) is consistent with the general argument that the frictional forces should be independent of the sign of $\dot{\omega}$. Hence, to lowest order the power against friction is proportional to μ^2 . Since $\mu \propto 1/\tau_{cycle}$ we expect that the asymptotic power against friction scales as Eq. (C.2) [15].

Appendix D. Endo-global cycle construction

The Endo-global cycle is constructed by combining two open strokes and two adiabats, that operate at a constant adiabatic speed. During the open strokes, the working medium dynamics is generated by the non-adiabatic master equation Eq. (A.1). This equation incorporates both the dissipative and unitary effects. It is exact for Markovian dynamics in the weak coupling regime and when the external driving is slow relative to the bath dynamics (see Ref. [36]). The condition of constant adiabatic speed, $|\mu| = \text{const}$, leads to protocols of the following form $\omega(t) = \omega_i / (1 - \omega_i \mu t)$, with initial frequency ω_i .

The unitary dynamics are given in terms of an operator basis in Liouville space, $\vec{v}(t) = \{\hat{H}(t), \hat{L}(t), \hat{C}(t), \hat{I}\}^T$. Here, $\hat{H}(t)$ is the Hamiltonian, Eq. (1),

$$\hat{L}(t) = \frac{\hat{P}^2}{2m} - \frac{1}{2}m\omega(t)^2 \hat{Q}^2$$

is the Lagrangian, and

$$\hat{C}(t) = \frac{\omega(t)}{2} (\hat{Q}\hat{P} + \hat{P}\hat{Q})$$

is the position-momentum correlation operator and \hat{I} is the identity operator. These operators completely determine the dynamics of the harmonic oscillator Gaussian state

(A.4), and give a clear physical interpretation of energy and coherence,

$$Coh = \frac{\sqrt{\langle \hat{L}(t) \rangle^2 + \langle \hat{C}(t) \rangle^2}}{\hbar\omega(t)} . \quad (D.1)$$

The solution for $\vec{v}(t)$ is given by [24]:

$$\frac{d\vec{v}}{dt} = \mathcal{U}_S(t) \vec{v}(0) , \quad (D.2)$$

with

$$\mathcal{U}_S(t) = \frac{1}{\kappa^2} \frac{\omega(t)}{\omega(0)} \begin{bmatrix} 4 - \mu^2 c & -\mu\kappa s & -2\mu(c-1) & 0 \\ -\mu\kappa s & \kappa^2 c & -2\kappa s & 0 \\ 2\mu(c-1) & 2\kappa s & 4c - \mu^2 & 0 \\ 0 & 0 & 0 & \kappa^2 \frac{\omega(0)}{\omega(t)} \end{bmatrix} \quad (D.3)$$

where $\kappa = \sqrt{4 - \mu^2}$ and $c = \cos(\kappa\theta(t))$, $s = \sin(\kappa\theta(t))$. The free propagation, governed by Eq. (D.3), mixes coherence and populations due to non-adiabatic driving [24].

In order to judge the performance for varying cycle-times, we construct different cycles with the same cycle frequencies, and vary $|\mu|$. The adiabatic parameter determines the stroke duration according to $\tau_{stroke} = \mu^{-1}(\omega_f - \omega_i) / (\omega_f \omega_i)$, where ω_f is the final frequency. The cycles are then propagated until convergence to the limit-cycle [48, 63], where the performance is evaluated.

Appendix E. Coherence measures

Coherence is associated with non-diagonal elements in the energy representation. This means that a state possessing coherence is non-stationary under the free Hamiltonian dynamics. There have been many proposals to quantify coherence [64]. In this context, two measures have been employed to analyze quantum heat engines: (i) Divergence, which becomes the difference between the energy and the von Neumann entropies [65, 66, 56, 35], and (ii) The algebraic definition of coherence, utilized here, Eq. (D.1).

Appendix F. Addition of pure dephasing

Pure dephasing is introduced during the adiabats of the Endo-global cycle to evaluate the importance of coherence in the engine operation. Such dephasing can be caused by noise in the driving field and weak measurement [67, 68, 55, 69]. A Lindbladian describing dephasing is added to the free dynamics. In the Heisenberg picture the master equation becomes

$$\frac{d\hat{X}(t)}{dt} = \frac{i}{\hbar} \left[\hat{H}(t), \hat{X}(t) \right] + \frac{\partial \hat{X}(t)}{\partial t} - \gamma_d \left[\hat{H}(t), \left[\hat{H}(t), \hat{X}(t) \right] \right] . \quad (F.1)$$

Here, the last term induces pure dephasing in the instantaneous energy basis, with a dephasing strength γ_d . We solve the dynamics, by representing the system in terms of the operator basis $\vec{v}(t) = \{\hat{H}(t), \hat{L}(t), \hat{C}(t), \hat{I}\}^T$, Cf. Appendix D. Substituting

Table G1. Cycle parameters

| Cycle parameter | Value (atomic units) |
|---|----------------------|
| Coupling strength, $\frac{ d ^2}{4\pi\epsilon_0\hbar c}$ | 0.05 |
| Stroke duration of the adiabatic expansion of the shortcut cycles | 5 |
| Stroke duration of the adiabatic compression of the shortcut cycles | 5 |

the basis operators into Eq. (F.1) we express the dynamics of $\vec{v}(t)$ in a matrix-vector notation

$$\frac{d}{dt}\vec{v}(t) = \omega(t) (\mu\mathcal{I} + \mathcal{M}) \vec{v}(t) \quad , \quad (\text{F.2})$$

where μ is the adiabatic parameter, \mathcal{I} is the identity matrix and \mathcal{M} is given by

$$\mathcal{M} = \begin{bmatrix} 0 & -\mu & 0 & 0 \\ -\mu & -4k_d\omega(t) & -2 & 0 \\ 0 & 2 & -4k_d\omega(t) & 0 \\ 0 & 0 & 0 & 1 \end{bmatrix} . \quad (\text{F.3})$$

Equation (F.2) is solved with a standard Runge-Kutta-Dormand-Prince propagator, leading to the system dynamics in the presence of pure-dephasing.

The reconstruction of the density operator, Eq. (A.4), from the $\{\hat{H}(t), \hat{L}(t), \hat{C}(t), \hat{I}\}$ operator basis assumes that the working medium is described by a generalized canonical state. Strictly, the dephasing dynamics, Eq. (F.1), does not conserve the Gaussian structure. Nevertheless, for the cases studied, where the coherence is relatively small, the Gaussian state is a valid representation.

Appendix G. Model parameters

The cycle parameters are described in Tables 1 and G1.

References

- [1] Sadi Carnot. *Réflexions sur la puissance motrice du feu et sur les machines propres à développer cette puissance*. Bachelier, 1824.
- [2] Peter Salamon, JD Nulton, Gino Siragusa, Torben Ravn Andersen, and Alfonso Limon. Principles of control thermodynamics. *Energy*, 26(3):307–319, 2001.
- [3] Bjarne Andresen, R Stephen Berry, Mary Jo Ondrechen, and Peter Salamon. Thermodynamics for processes in finite time. *Accounts of Chemical Research*, 17(8):266–271, 1984.
- [4] FL Curzon and B Ahlborn. Efficiency of a carnot engine at maximum power output. *American Journal of Physics*, 43(1):22–24, 1975.
- [5] II Novikov. The efficiency of atomic power stations (a review). *Journal of Nuclear Energy (1954)*, 7(1-2):125–128, 1958.
- [6] Massimiliano Esposito, Ryoichi Kawai, Katja Lindenberg, and Christian Van den Broeck. Quantum-dot carnot engine at maximum power. *Physical review E*, 81(4):041106, 2010.
- [7] Massimiliano Esposito, Ryoichi Kawai, Katja Lindenberg, and Christian Van den Broeck. Efficiency at maximum power of low-dissipation carnot engines. *Physical review letters*, 105(15):150603, 2010.
- [8] Robert Alicki. The quantum open system as a model of the heat engine. *Journal of Physics A: Mathematical and General*, 12(5):L103, 1979.
- [9] Ronnie Kosloff. Quantum thermodynamics: A dynamical viewpoint. *Entropy*, 15(6):2100–2128, 2013.
- [10] Sai Vinjanampathy and Janet Anders. Quantum thermodynamics. *Contemporary Physics*, 57(4):545–579, 2016.
- [11] Jochen Gemmer, Mathias Michel, and Günter Mahler. 4 brief review of pertinent concepts. In *Quantum Thermodynamics*, pages 37–58. Springer, 2004.
- [12] Xi Chen, A Ruschhaupt, Sebastian Schmidt, Adolfo del Campo, David Guéry-Odelin, and J Gonzalo Muga. Fast optimal frictionless atom cooling in harmonic traps: Shortcut to adiabaticity. *Physical review letters*, 104(6):063002, 2010.
- [13] Roie Dann, Ander Tobalina, and Ronnie Kosloff. Shortcut to equilibration of an open quantum system. *arXiv preprint arXiv:1812.08821*, 2018.
- [14] Tova Feldmann and Ronnie Kosloff. Quantum four-stroke heat engine: Thermodynamic observables in a model with intrinsic friction. *Physical Review E*, 68(1):016101, 2003.
- [15] G Francica, J Goold, and F Plastina. Role of coherence in the nonequilibrium thermodynamics of quantum systems. *Physical Review E*, 99(4):042105, 2019.
- [16] Francesco Plastina, A Alecce, TJG Apollaro, G Falcone, G Francica, Fernando Galve, N Lo Gullo, and Roberta Zambrini. Irreversible work and inner friction in quantum thermodynamic processes. *Physical review letters*, 113(26):260601, 2014.
- [17] Johannes Roßnagel, Samuel T Dawkins, Karl N Tolazzi, Obinna Abah, Eric Lutz, Ferdinand Schmidt-Kaler, and Kilian Singer. A single-atom heat engine. *Science*, 352(6283):325–329, 2016.
- [18] David von Lindenfels, Oliver Gräß, Christian T Schmiegelow, Vidyut Kaushal, Jonas Schulz, Mark T Mitchison, John Goold, Ferdinand Schmidt-Kaler, and Ulrich G Poschinger. Spin heat engine coupled to a harmonic-oscillator flywheel. *Physical Review Letters*, 123(8):080602, 2019.
- [19] Eitan Geva and Ronnie Kosloff. A quantum-mechanical heat engine operating in finite time. a model consisting of spin-1/2 systems as the working fluid. *The Journal of chemical physics*, 96(4):3054–3067, 1992.
- [20] Feng Wu, Lingen Chen, Shuang Wu, Fengrui Sun, and Chih Wu. Performance of an irreversible quantum carnot engine with spin 1/2. *The Journal of chemical physics*, 124(21):214702, 2006.
- [21] Carl M Bender, Dorje C Brody, and Bernhard K Meister. Quantum mechanical carnot engine. *Journal of Physics A: Mathematical and General*, 33(24):4427, 2000.
- [22] Ferdi Altintas. Comparison of the coupled quantum carnot and otto cycles. *Physica A: Statistical*

- Mechanics and its Applications*, 523:40–47, 2019.
- [23] Ronnie Kosloff and Tova Feldmann. Optimal performance of reciprocating demagnetization quantum refrigerators. *Physical Review E*, 82(1):011134, 2010.
- [24] Ronnie Kosloff and Yair Rezek. The quantum harmonic otto cycle. *Entropy*, 19(4):136, 2017.
- [25] Markus J Henrich, Florian Rempp, and Günter Mahler. Quantum thermodynamic otto machines: A spin-system approach. *The European Physical Journal Special Topics*, 151(1):157–165, 2007.
- [26] Johannes Roßnagel, Obinna Abah, Ferdinand Schmidt-Kaler, Kilian Singer, and Eric Lutz. Nanoscale heat engine beyond the carnot limit. *Physical review letters*, 112(3):030602, 2014.
- [27] Obinna Abah, Johannes Rosnagel, Georg Jacob, Sebastian Deffner, Ferdinand Schmidt-Kaler, Kilian Singer, and Eric Lutz. Single-ion heat engine at maximum power. *Physical review letters*, 109(20):203006, 2012.
- [28] Adolfo Del Campo, John Goold, and Mauro Paternostro. More bang for your buck: Superadiabatic quantum engines. *Scientific reports*, 4:6208, 2014.
- [29] Mathieu Beau, Juan Jaramillo, and Adolfo del Campo. Scaling-up quantum heat engines efficiently via shortcuts to adiabaticity. *Entropy*, 18(5):168, 2016.
- [30] Michele Campisi and Rosario Fazio. The power of a critical heat engine. *Nature communications*, 7:11895, 2016.
- [31] Barış Çakmak and Özgür E Müstecaplıoğlu. Spin quantum heat engines with shortcuts to adiabaticity. *Physical Review E*, 99(3):032108, 2019.
- [32] Obinna Abah and Mauro Paternostro. Shortcut-to-adiabaticity otto engine: A twist to finite-time thermodynamics. *Physical Review E*, 99(2):022110, 2019.
- [33] Selçuk Çakmak, Ferdi Altıntaş, Azmi Gençten, and Özgür E Müstecaplıoğlu. Irreversible work and internal friction in a quantum otto cycle of a single arbitrary spin. *The European Physical Journal D*, 71(3):75, 2017.
- [34] John PS Peterson, Tiago B Batalhão, Marcela Herrera, Alexandre M Souza, Roberto S Sarthour, Ivan S Oliveira, and Roberto M Serra. Experimental characterization of a spin quantum heat engine. *arXiv preprint arXiv:1803.06021*, 2018.
- [35] Patrice A Camati, Jonas FG Santos, and Roberto M Serra. Coherence effects in the performance of the quantum otto heat engine. *Physical Review A*, 99(6):062103, 2019.
- [36] Roie Dann, Amikam Levy, and Ronnie Kosloff. Time-dependent markovian quantum master equation. *Phys. Rev. A*, 98:052129, Nov 2018.
- [37] Roie Dann and Ronnie Kosloff. The inertial theorem. *arXiv preprint arXiv:1810.12094*, 2018.
- [38] Raam Uzdin, Amikam Levy, and Ronnie Kosloff. Equivalence of quantum heat machines, and quantum-thermodynamic signatures. *Physical Review X*, 5(3):031044, 2015.
- [39] James Klatzow, Jonas N Becker, Patrick M Ledingham, Christian Weinzetl, Krzysztof T Kaczmarek, Dylan J Saunders, Joshua Nunn, Ian A Walmsley, Raam Uzdin, and Eilon Poem. Experimental demonstration of quantum effects in the operation of microscopic heat engines. *Physical Review Letters*, 122(11):110601, 2019.
- [40] Harry JD Miller, Matteo Scandi, Janet Anders, and Martí Perarnau-Llobet. Work fluctuations in slow processes: quantum signatures and optimal control. *arXiv preprint arXiv:1905.07328*, 2019.
- [41] Goran Lindblad. On the generators of quantum dynamical semigroups. *Communications in Mathematical Physics*, 48(2):119–130, 1976.
- [42] Vittorio Gorini, Andrzej Kossakowski, and Ennackal Chandy George Sudarshan. Completely positive dynamical semigroups of n-level systems. *Journal of Mathematical Physics*, 17(5):821–825, 1976.
- [43] Robert Alicki and Ronnie Kosloff. Introduction to quantum thermodynamics: History and prospects. In Felix Binder, Luis A Correa, Christian Gogolin, Janet Anders, and Gerardo Adesso, editors, *Thermodynamics in the quantum regime*, Fundamental Theories of Physics. Springer, 2018.
- [44] Y Alhassid and RD Levine. Connection between the maximal entropy and the scattering theoretic

- analyses of collision processes. *Physical Review A*, 18(1):89, 1978.
- [45] Edwin T Jaynes. Information theory and statistical mechanics. *Physical review*, 106(4):620, 1957.
- [46] Edwin T Jaynes. Information theory and statistical mechanics. ii. *Physical review*, 108(2):171, 1957.
- [47] Yair Rezek and Ronnie Kosloff. Irreversible performance of a quantum harmonic heat engine. *New Journal of Physics*, 8(5):83, 2006.
- [48] Tova Feldmann and Ronnie Kosloff. Characteristics of the limit cycle of a reciprocating quantum heat engine. *Physical Review E*, 70(4):046110, 2004.
- [49] H Ralph Lewis Jr and WB Riesenfeld. An exact quantum theory of the time-dependent harmonic oscillator and of a charged particle in a time-dependent electromagnetic field. *Journal of Mathematical Physics*, 10(8):1458–1473, 1969.
- [50] Xi Chen, Erik Torrontegui, and Juan Gonzalo Muga. Lewis-riesenfeld invariants and transitionless quantum driving. *Physical Review A*, 83(6):062116, 2011.
- [51] Dionisis Stefanatos. Minimum-time transitions between thermal equilibrium states of the quantum parametric oscillator. *IEEE Transactions on Automatic Control*, 62(8):4290–4297, 2017.
- [52] E Torrontegui, I Lizuain, S González-Resines, A Tobalina, Andreas Ruschhaupt, R Kosloff, and Juan Gonzalo Muga. Energy consumption for shortcuts to adiabaticity. *Physical Review A*, 96(2):022133, 2017.
- [53] Ander Tobalina, Joseba Alonso, and Juan G Muga. Energy consumption for ion-transport in a segmented paul trap. *New Journal of Physics*, 20(6):065002, 2018.
- [54] Andrew Silberfarb, Poul S Jessen, and Ivan H Deutsch. Quantum state reconstruction via continuous measurement. *Physical review letters*, 95(3):030402, 2005.
- [55] Thomas Konrad, Andreas Rothe, Francesco Petruccione, and Lajos Diósi. Monitoring the wave function by time continuous position measurement. *New Journal of Physics*, 12(4):043038, 2010.
- [56] Tova Feldmann and Ronnie Kosloff. Transitions between refrigeration regions in extremely short quantum cycles. *Physical Review E*, 93(5):052150, 2016.
- [57] Ronnie Kosloff and Amikam Levy. Quantum heat engines and refrigerators: Continuous devices. *Annual Review of Physical Chemistry*, 65:365–393, 2014.
- [58] Luis A Correa, José P Palao, Gerardo Adesso, and Daniel Alonso. Performance bound for quantum absorption refrigerators. *Physical Review E*, 87(4):042131, 2013.
- [59] Karl Heinz Hoffmann, Josef Maximilian Burzler, and Sven Schubert. Endoreversible thermodynamics. 1997.
- [60] Ken Funo, Neill Lambert, Bayan Karimi, Jukka Pekola, Yuta Masuyama, and Franco Nori. Speeding-up a quantum refrigerator via counter-diabatic driving. *arXiv preprint arXiv:1905.03480*, 2019.
- [61] HC Andersen, I Oppenheim, Kurt E Shuler, and George H Weiss. Exact conditions for the preservation of a canonical distribution in markovian relaxation processes. *Journal of Mathematical Physics*, 5(4):522–536, 1964.
- [62] Heinz-Peter Breuer, Francesco Petruccione, et al. *The theory of open quantum systems*. Oxford University Press on Demand, 2002.
- [63] Andrea Insinga, Bjarne Andresen, Peter Salamon, and Ronnie Kosloff. Quantum heat engines: Limit cycles and exceptional points. *Physical Review E*, 97(6):062153, 2018.
- [64] Tillmann Baumgratz, Marcus Cramer, and Martin B Plenio. Quantifying coherence. *Physical review letters*, 113(14):140401, 2014.
- [65] Göran Lindblad. Expectations and entropy inequalities for finite quantum systems. *Communications in Mathematical Physics*, 39(2):111–119, 1974.
- [66] Raam Uzdin and Saar Rahav. Global passivity in microscopic thermodynamics. *Physical Review X*, 8(2):021064, 2018.
- [67] Tova Feldmann and Ronnie Kosloff. Quantum lubrication: Suppression of friction in a first-principles four-stroke heat engine. *Physical Review E*, 73(2):025107, 2006.
- [68] Amikam Levy, E Torrontegui, and Ronnie Kosloff. Action-noise-assisted quantum control.

Physical Review A, 96(3):033417, 2017.

- [69] Howard M Wiseman and Gerard J Milburn. *Quantum measurement and control*. Cambridge university press, 2009.